Heliyon 10 (2024) e32158

Contents lists available at ScienceDirect

Heliyon

journal homepage: www.cell.com/heliyon

Research article

Identification of PATL1 as a prognostic and immunotherapeutic predictive factor for nasal-type natural killer/T-cell lymphoma and head and neck squamous cell carcinoma

Wen Yang [a,b], Cong Peng [c], Zhengyang Li [c], Wenxiu Yang [a,b,*]

[a] Department of Pathology, Affiliated Hospital of Guizhou Medical University, China
[b] Department of Pathology, Guizhou Medical University, China
[c] Department of Otolaryngology, Guizhou Provincial People's Hospital, China

ARTICLE INFO

Keywords:
PATL1
Nasal-type natural killer/T-cell lymphoma
Head and neck squamous cell carcinoma
Prognosis
Immunotherapy

ABSTRACT

This research examines the function of protein associated with topoisomerase II homolog 1 (*PATL1*) in nasal-type natural killer/T-cell lymphoma (NKTCL) and head and neck squamous cell carcinoma (HNSCC). We analyzed bulk RNA-seq data from NKTCL, nasal polyps, and normal nasal mucosa, identifying 439 differentially expressed genes. Machine learning algorithms highlighted *PATL1* as a hub gene. *PATL1* exhibited significant upregulation in NKTCL and HNSCC tumor samples in comparison to normal tissues, showing high diagnostic accuracy (AUC = 1.000) for NKTCL. Further analysis of local hospital data identified *PATL1* as an independent prognostic risk factor for NKTCL. Data analysis of TCGA and GEO datasets revealed that high *PATL1* expression correlated with poorer prognosis in HNSCC patients ($p < 0.05$). We also constructed a *PATL1*-based nomogram, which emerged as an independent prognostic predictor for HNSCC after addressing missing values. Additionally, we found a strong correlation between *PATL1* and various immune cell infiltrates (e.g., activated.CD4 T cell), and a significant association with the expression of 37 immune checkpoints genes (e.g., *CTLA4*, *PDCD1*) and 20 N6-methyladenosine-related genes (e.g., *ZC3H13*, *METTL3*) (all $p < 0.05$). Both TCIA and TIDE algorithms suggested that *PATL1* could potentially predict immunotherapy efficacy ($p < 0.05$). Cellular experiments demonstrated that transfection with a silencing plasmid of *PATL1* significantly inhibited the malignant behaviors of SNK6 and FaDu cell lines($p < 0.05$). In conclusion, our findings suggest that *PATL1* may serve as a valuable prognostic and predictive biomarker in NKTCL and HNSCC, highlighting its significant role in these cancers.

1. Introduction

In recent years, malignant lymphoma has emerged as a prevalent form of cancer on a global scale, with 544,352 instances of Hodgkin lymphoma and 83,087 instances of non-Hodgkin lymphoma reported in 2020 [1]. Nasal-type natural killer/T-cell lymphoma (NKTCL) is an uncommon form of non-Hodgkin lymphoma that mainly affects the upper respiratory system, such as the nasal cavity, nasopharynx, larynx, and upper passages. Although the incidence of NKTCL is not high worldwide, it is relatively common in southeast asia [2]. NKTCL commonly manifests as worsening symptoms in the upper respiratory tract, including blockage in the nose, runny

* Corresponding author. Department of Pathology, Affiliated Hospital of Guizhou Medical University, China.
E-mail address: yangwenxiu2022@163.com (W. Yang).

https://doi.org/10.1016/j.heliyon.2024.e32158
Received 11 December 2023; Received in revised form 17 May 2024; Accepted 29 May 2024
Available online 31 May 2024

nose, pain in the throat and larynx, coughing, and difficulty breathing, and is strongly linked to Epstein-Barr virus (EBV) infection [3]. Notably, EBV is also a significant etiological factor for nasopharyngeal carcinoma, a distinct type of head and neck cancer [4]. Additionally, since NKTCL and head and neck squamous cell carcinoma (HNSCC) both manifest in the head and neck area, there could be similarities in lifestyle choices or environmental influences, like smoking and drinking, that are associated with different forms of cancers in this specific region. Additionally, these cancers may exhibit similar clinical symptoms early on and may share molecular pathways and therapeutic targets, such as *p53* and *MAPK* [5,6]. Therefore, despite the clear differences in origin, pathogenesis, and treatment strategies between NKTCL and HNSCC, their anatomical and some clinical similarities necessitate consideration of their potential interconnections in clinical practice and research. Moreover, the cross-disciplinary studies of these diseases may provide new perspectives and possibilities for future cancer treatment strategies.

Despite the considerable progress made in cancer treatment approaches in recent years, there are still many obstacles to overcome, especially the absence of precise and reliable biomarkers for detecting, predicting, and monitoring treatment effectiveness [7,8]. Early cancer diagnosis plays a critical role in influencing treatment outcomes and patient prognosis. However, current technologies for early tumor diagnosis still face many limitations and challenges. Bioinformatics technology can analyze molecular information from tumor tissue and fluid samples to identify and validate potential biomarkers [9–11]. These biomarkers have high specificity and sensitivity and can serve as important indicators for early tumor diagnosis and prognosis [12,13]. Furthermore, bioinformatics technology enables the comprehensive analysis and integration of biomarkers, leading to a better comprehension of tumor formation and progression mechanisms and offering assistance for precision medicine [14,15]. In this context, bioinformatics technology offers new directions and possibilities for early tumor diagnosis and prognosis. Furthermore, bioinformatics research explores the common molecular biological mechanisms across different diseases, providing new perspectives and deep insights for medical research [16]. However, studies using bioinformatics to screen and predict prognostic biomarkers for NKTCL and HNSCC are currently limited.

This research utilized transcriptome sequencing to analyze gene expression levels in NKTCL, nasal polyps, and normal nasal mucosa tissue and employed machine learning algorithms to pinpoint crucial genes. We also explored the prognostic value of hub gene, protein associated with topoisomerase II Homolog 1(*PATL1)* for NKTCL using data of 55 patients with from our local hospital. Furthermore, we examined predictive significance of *PATL1* for HNSCC in terms of prognosis and response to immunotherapy by analyzing data from TCGA and t GEO databases, and assessing its relationship with immune cell infiltration. *In vitro* studies were also carried out to confirm the function of *PATL1* in both NKTCL and HNSCC. Our data and results demonstrate that *PATL1* may serve as a novel diagnostic and therapeutic target for the treatment of NKTCL and HNSCC.

2. Materials and methods

2.1. Data preparation

For this research, RNA sequencing data from three instances of NKTCL, three instances of nasal polyps, and three instances of normal nasal mucosa tissue were gathered from the Guizhou Provincial People's Hospital as part of the data preparation process. The clinical information for these cases can be found in Table 1. Furthermore, a retrospective analysis was conducted on 55 instances of NKTCL patients at the hospital affiliated with Guizhou Medical University. Table 2 contains the clinical data for these cases. Follow-up for these patients was conducted July 1, 2023. Patients diagnosed with HNSCC, had their clinical information and RNA sequencing data collected from the TCGAand GEO databases. After excluding cases with a survival time of less than 30 days, a total of 500 cases from TCGA-HNSCC and 270 cases from GSE65858 were merged after batch effect removal to create a training set. An additional 97 cases from GSE41613 were used as a validation set. The clinical information for training set and validation set can be found in Table 3 and Table 4, respectively. Our entire work was presented in Fig. 1.

2.2. Machine learning techniques to identify hub genes in NKTCL

Differential expression analysis was carried out with the "limma" package to detect genes that were expressed differentially across different samples. The criteria set required an absolute log fold change (logFC) of at least 2 and an adjusted p-value of less than 0.05, which resulted in the identification of 443 DEGs. To obtain hub genes in the progression of NKTCL, a machine learning-based approach was employed for further selection. The initial approach involved using the "glmnet" package to implement the least absolute shrinkage and selection operator (LASSO) technique on the 443 differentially expressed genes (DEGs). During this process, the optimal penalty parameter (λ) was determined through ten-fold cross-validation, aiming to select the model with the lowest deviation anomaly probability. Only genes with non-zero coefficients were retained following regression analysis. Following, the support vector machine - recursive feature elimination (SVM-RFE) algorithm was implemented using the "e1071″, "kernlab", and "caret" packages. Evaluating the predictive performance of the model involved focusing on the root mean square error (RMSE) and selecting the number of features

Table 1
Clinical features of patients with nasal-type natural killer/T-cell lymphoma (NKTCL), nasal polyps, and nasal septum deviation.

Clinical features	NKTCL(n = 3)	nasal polyps(n = 3)	normal nasal mucosa tissue(n = 3)
Age at diagnosis(years)	67,39,58	42,20,55	29,40,52
Gender (Male/Female)	3/0	2/1	3/0
Stage(I-II/III-IV)	2/1	/	/

Table 2
Clinical features of 55 patients with NKTCL.

Clinical features	
Age at diagnosis(years)	45.69 ± 15.41
Gender (Male/Female)	37/18
Stage(I-II/III-IV)	41/14
Fever (Yes/No)	22/33
LDH level (High/normal)	18/37
White blood cell count (Decreased/normal)	10/45
EBV load($\leq$/$>6.1 \times 10^7$ copies/mL)	40/15
PATL1(negative/positive)	38/17

Table 3
Clinical features of patients with head and neck squamous carcinoma (HNSCC) before and after multiple imputation in the Cancer Genome Atlas (TCGA) and GSE65858 datasets.

Clinical features	Before multiple imputation	After multiple imputation
Age at diagnosis(<60/≥60/NA)	415/377/1	416/377
Gender (Male/Female)	605/188	605/188
Grade(G1/G2/G3/G4/NA)	63/308/123/7/292	91/478/194/30
Stage(I/II/III/IV/NA)	44/111/119/445/74	53/129/137/474
HPV16(positive/negative/NA)	101/283/409	197/596
Lymph deneckdissection (Yes/No/NA)	424/96/273	646/147
Treatment(surgery/radiation/chemotherapy/NA)	98/39/58/598	427/139/227
radiationtherapy (Yes/No/NA)	270/143/380	520/273
Margin status(close/positive/negative/NA)	49/60/354/330	85/122/586
Alcoholhistory exposures (Yes/No/NA)	587/206	587/206
smokeless (Yes/No/NA)	59/444/290	93/700

Table 4
Clinical features of patients with HNSCC in GSE41613 datasets.

Variable	Number of samples
Age at diagnosis (<60/≥60)	50/47
Gender(Male/Female)	66/31
Stage(I-II/III-IV)	41/56
HPV16(negative)	97

at the point where RMSE was lowest. Finally, the intersection of genes selected by LASSO and SVM-RFE was determined to be the hub genes for NKTCL.

2.3. Biological function analysis

Analysis of biological function involved a comprehensive examination of the 443 DEGs utilizing the "clusterProfiler" and "DOSE" packages. These instruments enabled in-depth functional annotation and pathway examination using gene ontology (GO), kyoto encyclopedia of genes and genomes (KEGG), and disease ontology (DO) assessments. Furthermore, HNSCC datasets, utilized the "GSVA" package to explore pathways linked to *PATL1*.

2.4. Immunological analysis

The single-sample gene set enrichment analysis (ssGSEA) algorithm, implemented via the "GSVA" package, was used to evaluate immune function and immune cell infiltration levels across all datasets. The relationship between the *PATL1* expression and immune function or immune cells was analyzed using the "ggcor" package. Additionally, the "ggpubr" package enabled the examination of the association between *PATL1*, immune checkpoint genes, and N6-methyladenosine (m6A)-related genes. *PATL1*'s ability to predict the effectiveness of immunotherapy was evaluated through the utilization of the tumor immune dysfunction and exclusion (TIDE) and the cancer immunome atlas (TCIA) algorithms. Finally, the "ggplot2" (version 3.4.2) and "ggpubr" (version 0.4.0) packages were used to depict differences between groups and the disparities in immunotherapy scores between high and low *PATL1* expression groups, respectively.

2.5. Immunohistochemistry

In short, tissue sections embedded in paraffin were treated to remove paraffin and restore hydration, then underwent antigen

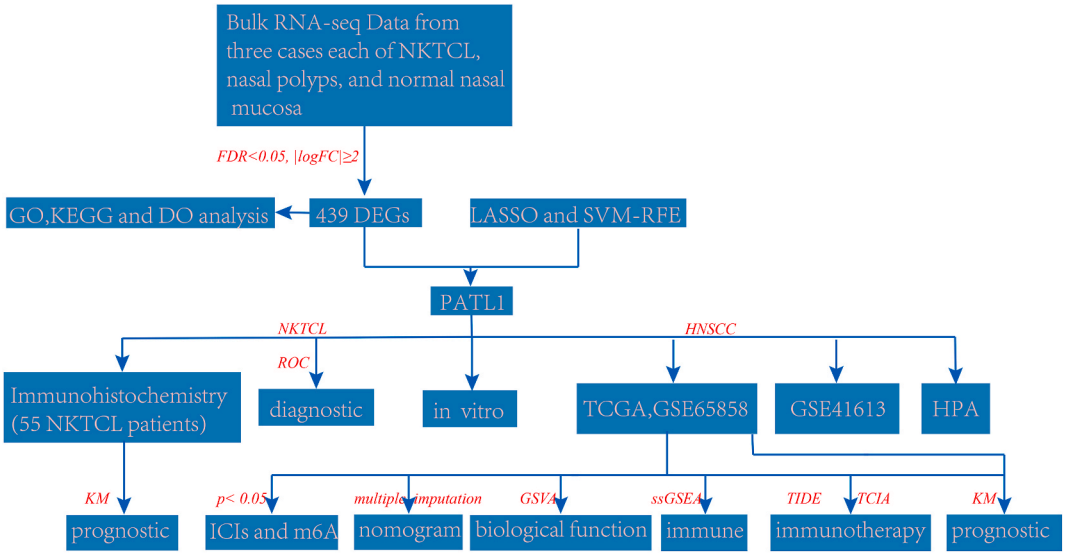

Fig. 1. The study flowchart. PATL1*:* protein associated with topoisomerase II homolog 1, NKTCL: Nasal-type Natural Killer/T-cell Lymphoma, GO: Gene Ontology, LASSO: Least Absolute Shrinkage and Selection Operator, SVM-RFE: Support Vector Machine-Recursive Feature Elimination, ROC: Receiver Operating Characteristic, HNSCC: Head and Neck Squamous Cell Carcinoma, HPA: Human Protein Atlas, KM: Kaplan-Meier, FDR: False discovery rate, KEGG: Kyoto Encyclopedia of Genes and Genomes, DO: Disease Ontology. DEGs, differentially expressed genes, TCGA, The Cancer Genome Atlas, ssGSEA, single-sample gene-set enrichment analysis, TCIA, The Cancer Immunome Atlas, TIDE, Tumor Immune Dysfunction and Exclusion.

retrieval and inhibition of natural peroxidase activity. Following that, the segments were exposed to a primary antibody targeting *PATL1* (Abcam, Cambridge, MA, USA) at a concentration of 1:100 and kept at 4 °C for the entire night. Following the wash, the portions were exposed to a secondary antibody conjugated with horseradish peroxidase (HRP) at room temperature for 30 min. Afterward, he segments were displayed by utilizing 3,3′-diaminobenzidine (DAB) substrate, followed by a hematoxylin counterstain, and then they were mounted. Two independent pathologists evaluated the *PATL1* expression level without knowledge of the patients' clinical information. Staining intensity was assessed using a 0–3 scale (0 = absent, 1 = faint, 2 = medium, 3 = intense), while the percentage of cells with positive staining was evaluated on a 0–4 scale (0 = <5 %, 1 = 5–25 %, 2 = 26–50 %, 3 = 51–75 %, 4 = >75 %).

2.6. Cell culture and plasmid transfection

The NKTCL cell line SNK6 was obtained from Yiyan Biotech, in Shanghai, while the HNSCC cell line FaDu was acquired from the American Type Culture Collection (ATCC). The SNK6 cell line was grown in RPMI-1640 medium with 20 % fetal bovine serum (FBS), IL2 (1000U/ml), and penicillin-streptomycin (PS), obtained from Gibco, United States. FaDu cells were cultured in both DMEM and RPMI-1640 media, each enriched with 10 % FBS, also from Gibco, USA. The two cell cultures were moved to T25 flasks and kept in a stable temperature incubator at 37 °C with 5 % carbon dioxide in a humid environment. When cells reached 90 % confluency, they well detached using trypsin, counted, and then placed in six-well plates at a density of 2.0×10^5 cells per well. When confluency reached about 70 %, transfection procedures commenced using the Lipofectamine™ 3000 reagent kit from Thermo Scientific, USA. Transfections included siRNA targeting *PATL1* (5′- GGAUGAAGAUGAAGAUGCAUU-3′) and a negative control plasmid (5′- UUCUCCGAACGUGUCACGUTT-3′), both sourced from Hesheng Biotech, Shanghai.

2.7. Western blot

Following a 48-h period of plasmid transfection, various cell types were collected and lysed with RIPA lysis buffer that included protease and phosphatase inhibitors. After centrifuging the lysates at 12,000 rpm for 15 min, at 4 °C, the liquid portion was gathered. supernatant was collected. Protein concentration was quantified using the BCA Protein Assay Kit. Following this, 10 μL of protein solution from each sample was applied to SDS-PAGE gels, and electrophoresis was carried out at a steady 70 V until proteins moved into the resolving gel, at which time the voltage was raised to 110 V until the marker bands were clearly distinguished. After electrophoresis, the proteins were moved to a PVDF membrane using 85 V for 60 min. The membrane was subsequently cut based on athe molecular weight of the proteins and then covered with 10 % skim milk at ambient temperature for 1–2 h. Antibodies targeting *PATL1* (1:2000) and *GAPDH* (1:2000), both purchased from Abcam, were used and left to incubate overnight at 4 °C. Afterward, the sample was incubated at room temperature for 2 h with secondary antibody, Goat Anti-Rabbit IgG (1:2000) from Abcam, which was conjugated with horseradish peroxidase. Protein bands were visualized using an ECL chemiluminescence reagent and exposed bands were quantitatively analyzed for relative gray scale intensity using Image J software. All the original blot gel images were presented in

Supplementary Fig. 1.

2.8. CCK-8 assay

Log-phase SNK6 and FaDu cells were harvested using trypsin digestion and counted. 2000 cells were placed in each well of a 96-well plate for the CCK-8 assay. Each well was filled with 100 μL of complete culture medium containing the cell suspension. Cell viability was assessed by measuring the optical density (OD) of each well at day 0, 1, 2, and 3 post-seeding. 10 μL of CCK-8 reagent was added to every well in order to perform the assay. Afterward, the dish was placed in an incubator set at a temperature of 37 °C for a duration of 2 h. Cell viability was determined by measuring absorbance at 450 nm with a microplate reader The resulting data were used to plot the cell growth curve.

2.9. Cell apoptosis assay

Using the Annexin V-APC/7-AAD dual staining method, cells from the NC, siNC, and si-P*ATL1* groups were harvested using trypsin digestion without EDTA and collected into EP tubes. After centrifugingthe cells at a speed of 1000 rpm for 5 min, the liquid portion was removed, and the cells were rinsed with PBS once. After counting, 2.5×10^5 cells were resuspended, washed again with PBS, and the supernatant discarded. Afterward, the cells were suspended again in 100 μL of Annexin V Binding Buffer. 2.5 μL of Annexin V-APC and 2.5 μL of 7-AAD staining solution were introduced to the cell suspension. After gently swirling the mixture, it was gently left to incubate in the dark at room temperature for 15 min prior to flow cytometry analysis.

2.10. Transwell migration assay

The cells were taken out of the incubator and the liquid used for growing them was thrown away. The cells were washed 1–2 times with PBS and then treated with an appropriate amount of trypsin to detach them. After detachment, complete medium was added to stop the trypsinization. Cells were then collected in EP tubes and centrifuged at 1200 rpm for 5 min. The supernatant was removed, and cells were resuspended in PBS, followed by another centrifugation and a repeat of the washing step. Following enumeration, the concentration of cells was modified to a range of $(1–5) \times 10^5$ cells per milliliter. Cells in a 200 μL suspension were placed in the top compartment of the transwell, with 300 μL of medium with 5 % FBS added to the bottom compartment of a 24-well plate. The assembly was incubated for 24 h under standard conditions. After the incubation period, the transwell inserts were taken out, and the cells adhered to the inner surface of the insert were removed using a cotton swab. The cells on the opposing side were treated with 4 % paraformaldehyde at room temperature for 10–20 min, then rinsed with distilled water for 2 min, followed by a fresh water change and

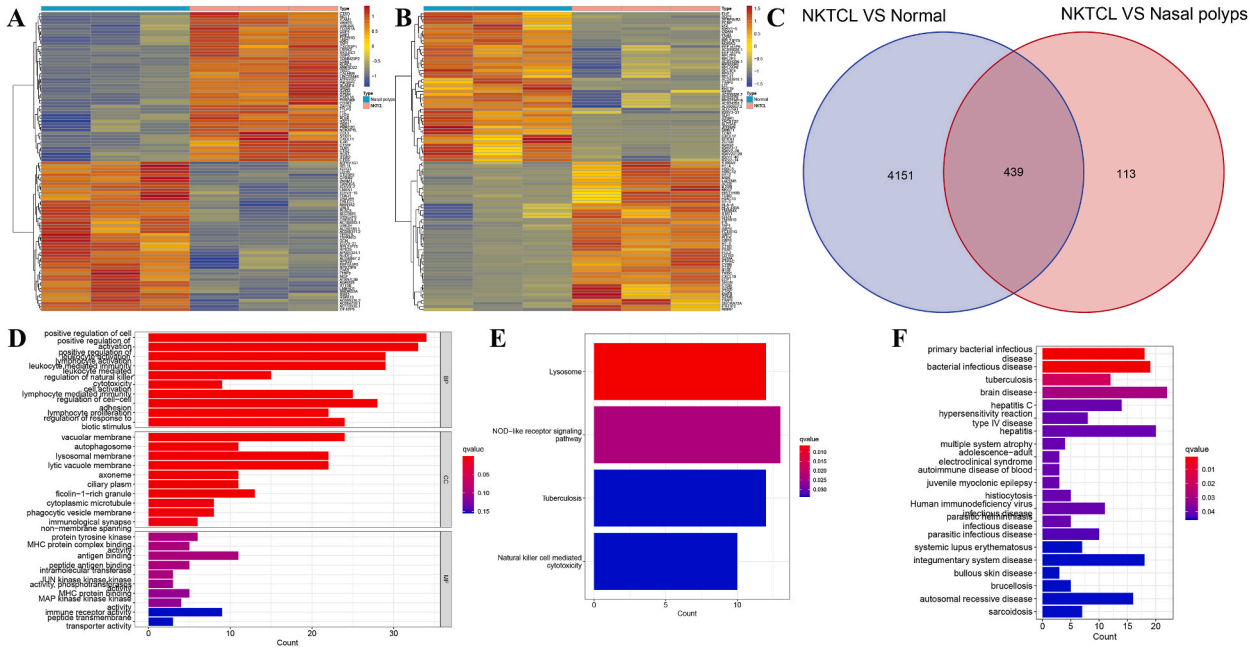

Fig. 2. Differential gene expression and pathway enrichment analysis in NKTCL, nasal polyps, and normal nasal mucosa. (A–B) Heatmap plots showing the differentially expressed genes between NKTCL and nasal polyps (A), and between NKTCL and normal nasal mucosa (B). (C) Venn diagram illustrating the intersection of differentially expressed genes in both comparisons, resulting in 439 genes. (D–F) GO(D), and KEGG pathway (E), DO (F)enrichment analysis of the 439 intersected genes. NKTCL: Nasal-type Natural Killer/T-cell Lymphoma, GO: Gene Ontology, KEGG: Kyoto Encyclopedia of Genes and Genomes, DO: Disease Ontology.

another 2-min rinse.Afterward, the cells were treated with crystal violet and left for 10–15 min. After thorough rinsing with tap water, the cells were observed and photographed for analysis.

2.11. Statistical analysis

Cell experiments were conducted thrice for validation. Data analysis was performed with R software (v4.2.0) and graphpad prism (v 9.0). Continuous variables were expressed as mean ± standard deviation, while categorical variables were presented as frequencies and percentages. Continuous variables were compared between two groups using the independent *t*-test for normally distributed data and the wilcoxon rank-sum test for non-normally distributed data. ANOVA was used for comparing more than two groups. Categorical variables were compared using Pearson's chi-squared test or Fisher's exact test. Spearman's rank correlation was utilized for conducting correlation analyses. Missing data were imputed using the multiple imputation method via the "mice" package. Unicox and multivariable Cox regression were used to assess the predictive importance of nomograms and additional clinical factors, displaying outcomes as hazard ratios (HRs) along with 95 % confidence intervals (CIs). Furthermore, Kaplan-Meier survival curves were analyze using log-rank tests to compare patients with varying levels of *PATL1* expression. Statistical tests were conducted with a two-sided approach, with significance defined as p-values <0.05.

3. Results

3.1. Biological analysis of DEGs in NKTCL

To assess the consistency of the samples, we employed principal component analysis (PCA) on the transcriptome sequencing data. The results demonstrated that samples within the same group clustered closely together, whereas there was a significant separation between different groups, indicating good consistency among the samples (Supplementary Fig. 2). Further, to differentiate between NKTCL and nasal polyps, we performed a gene expression analysis of NKTCL, nasal polyps, and normal nasal mucosa. We identified 552 and 4590 differentially expressed genes between nasal NKTCL and nasal polyps and between NKTCL and normal nasal mucosa, respectively (Fig. 2A and B). We then intersected these genes and identified 439 genes that were differentially expressed in both comparisons (Fig. 2C). Enrichment analysis was performed on these genes using GO, KEGG, and DO, showing enrichment in pathways related to inflammation and the immune system such as leukocyte mediated immunity, regulation of natural killer cell activation, and natural killer cell mediated cytotoxicity (Fig. 2D and E). Significantly, the analysis of gene enrichment revealed that these genes were enriched in infectious and immune disorders, such as primary bacterial infections and human immunodeficiency virus infections (Fig. 2F). NKTCL is linked to specific disease-causing agents like EBV, human T-cell lymphotropic virus type 1, and influenza virus [17,18]. These pathogens can induce inflammation and activate immune cells, promoting tumor cell proliferation and infiltration. In addition, changes in immune function may also be associated with NKTCL development. Those with HIV are more likely to develop extranodal NK/T-cell lymphoma compared to the general population [19,20]. HIV infection can cause immune system damage and

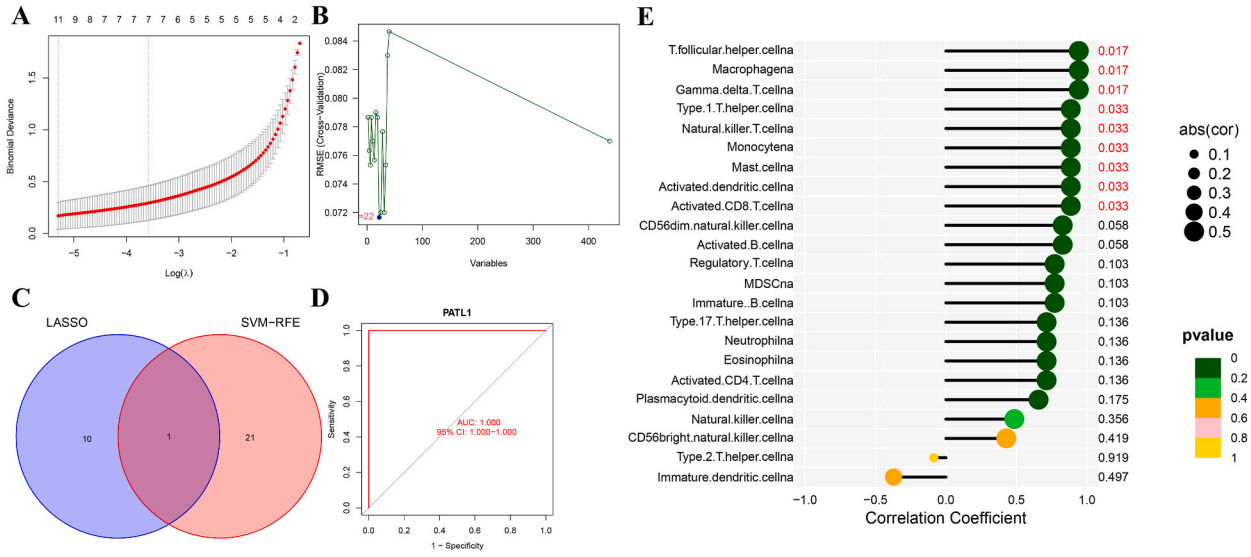

Fig. 3. Identification of PATL1 as a hub gene using LASSO and SVM-RFE. (A–B) LASSO (A) and SVM-RFE (B) were used to screen the 439 differentially expressed genes. (C) Venn diagram showing the intersection of the two methods, identifying PATL1 as a hub gene. (D) The ROC curve to confirm accurate value of PATL1expression in diagnosis (AUC = 1.000). (E) The lollipop chart displaying the correlation between PATL1 expression and the abundance of various immune cell infiltrates. LASSO: Least Absolute Shrinkage and Selection Operator, SVM-RFE: Support vector machine-recursive feature elimination, ROC: Receiver operating characteristic, AUC: Area under the curve.

immunosuppression, increasing the risk of NKTCL. Overall, infectious diseases and changes in immune function may be associated with the occurrence and development of NKTCL. However, further research is needed to explore and confirm the specific mechanisms and relationships involved.

3.2. Prognostic predictive value of PATL1 for NKTCL

To identify biomarkers for predicting tumor diagnosis, prognosis, or treatment [21–23], we used LASSO and SVM-RFE to analyze 439 DEGs(Fig. 3A and B). Through the intersection of the two methods, we identified the *PATL1* as a hub gene (Fig. 3C). The receiver operating characteristic (ROC) curve was utilized to validate precise *PATL1* expression values in diagnosis with an AUC of 1.000) (Fig. 3D). Given the important function of immune cells in the tumor microenvironment, we conducted a more in-depth examination of the correlation between *PATL1* expression and the infiltration of immune cells in NKTCL. Using the ssGSEA method, it was discovered that *PATL1* has a positive correlation with the presence of nine different immune cell types, such as T follicular helper cells, macrophages, gamma delta T cells, and natural killer T (NKT) cells ($p < 0.05$) (Fig. 3E), reinforcing the research potential of *PATL1* in NKTCL given its close association with NK cells and T cells. To further investigate the prognostic value of *PATL1* in NKTCL, we performed immunohistochemical analysis on pathological sections of 55 patients (Fig. 4A and B), and found that those with positive expression had poorer prognosis (Fig. 4C). Drawing on previous literature [24,25], we collected some clinical parameters of NKTCL and selected a threshold of $>6.1 \times 10^7$ copies/mL for the EBV DNA load as a categorical variable. Following univariate and multivariate Cox regression analysis, we discovered that both *PATL1* expression and elevated EBV DNA levels in serum ($>6.1 \times 10^7$ copies/mL) were independent prognostic indicators for NKTCL (Fig. 4D). In summary, our study suggests that *PATL1* is involved in the

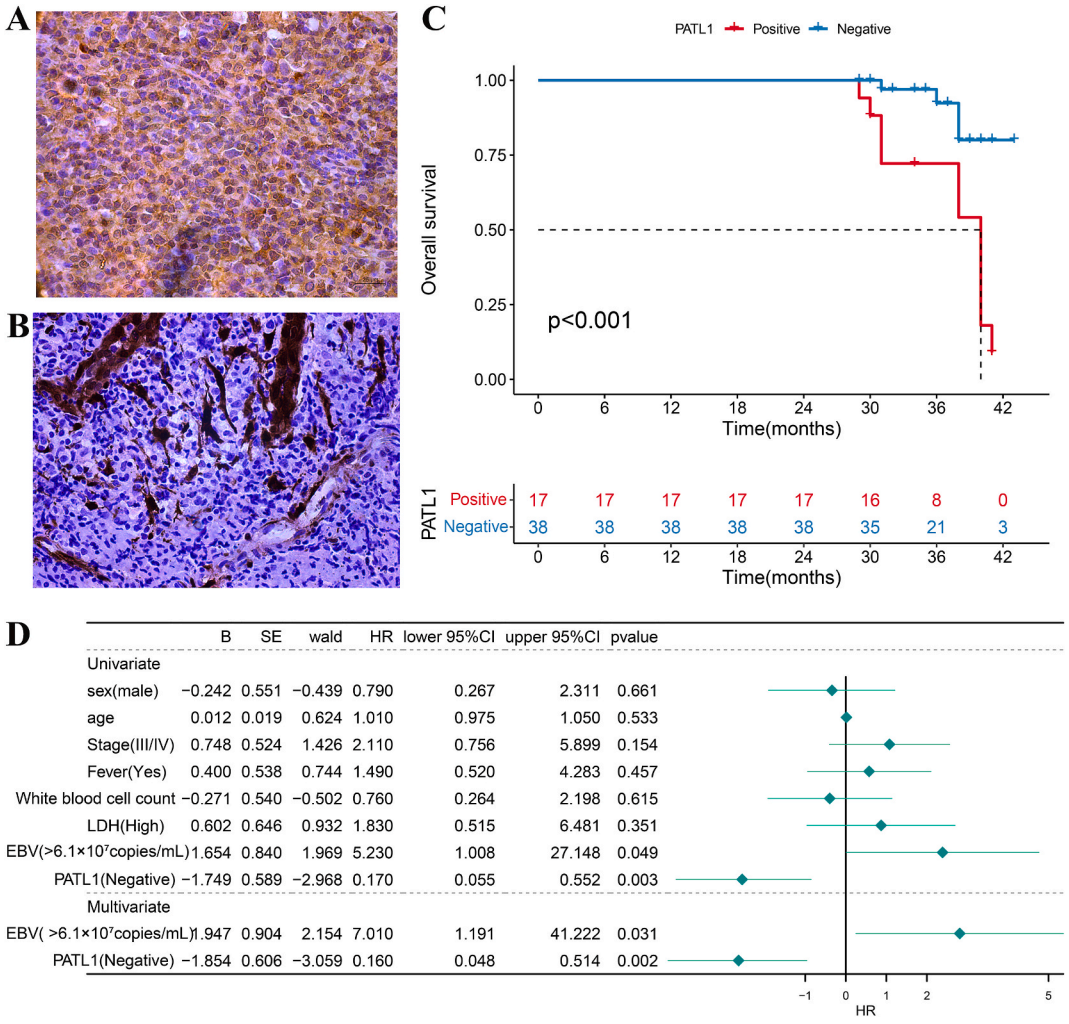

Fig. 4. Prognostic value of PATL1 in NKTCL. (A–B) Immunohistochemical analysis of pathological sections from 55 patients. (C) Kaplan-Meier survival analysis showing that patients with positive PATL1 expression have a poorer prognosis. (D) Univariate and multivariate Cox regression analysis indicating that PATL1 is an independent prognostic factor for NKTCL.

progression of NKTCL and can serve as a prognostic predictor for this disease.

3.3. Prognostic predictive value of PATL1 for HNSCC

NKTCL and nasopharyngeal carcinoma are both head and neck tumors, and a previous study has examined the prognostic value of these cancers using the TCGA and GEO databases [26]. In order to further strengthen our research findings, we analyzed the role of *PATL1* in HNSCC using the same method. Elevated levels of *PATL1* were detected in different tumor tissues, such as HNSCC, in comparison to normal tissues (Fig. 5A). Additionally, in HNSCC, the expression of *PATL1* showed no significant differences between gender and age groups, but it did exhibit significant differences in G and TNM stages($p < 0.05$) (Fig. 5B). In the HPA database, the expression of *PATL1* was positive in tumor tissues of HNSCC, but not in normal tissues (Fig. 5C). These results suggest that *PATL1* may function as an oncogene in HNSCC. Additionally, our hypothesis, was validated through survival analysis, which revealed that patients with elevated expression levels had notably poorer prognoses compared to those with lower expression levels in both the training and test sets (Fig. 5D–E). Several bioinformatics research projects have developed nomograms using the levels of target genes' expression to enhance the accuracy of predicting patient outcomes for healthcare professionals [27,28]. Therefore, we also constructed a nomogram based on the expression level of *PATL1*(Fig. 6A). We utilized multiple imputation methods to fill in missing values, with the distributions of each variable before and after imputation presented in Supplementary Fig. 3. Additional examination showed that the developed nomogram is a standalone predictor for forecasting the outcome of HNSCC (Fig. 6B–D). In summary, the results of our study indicate that *PATL1* plays an important role in HNSCC.

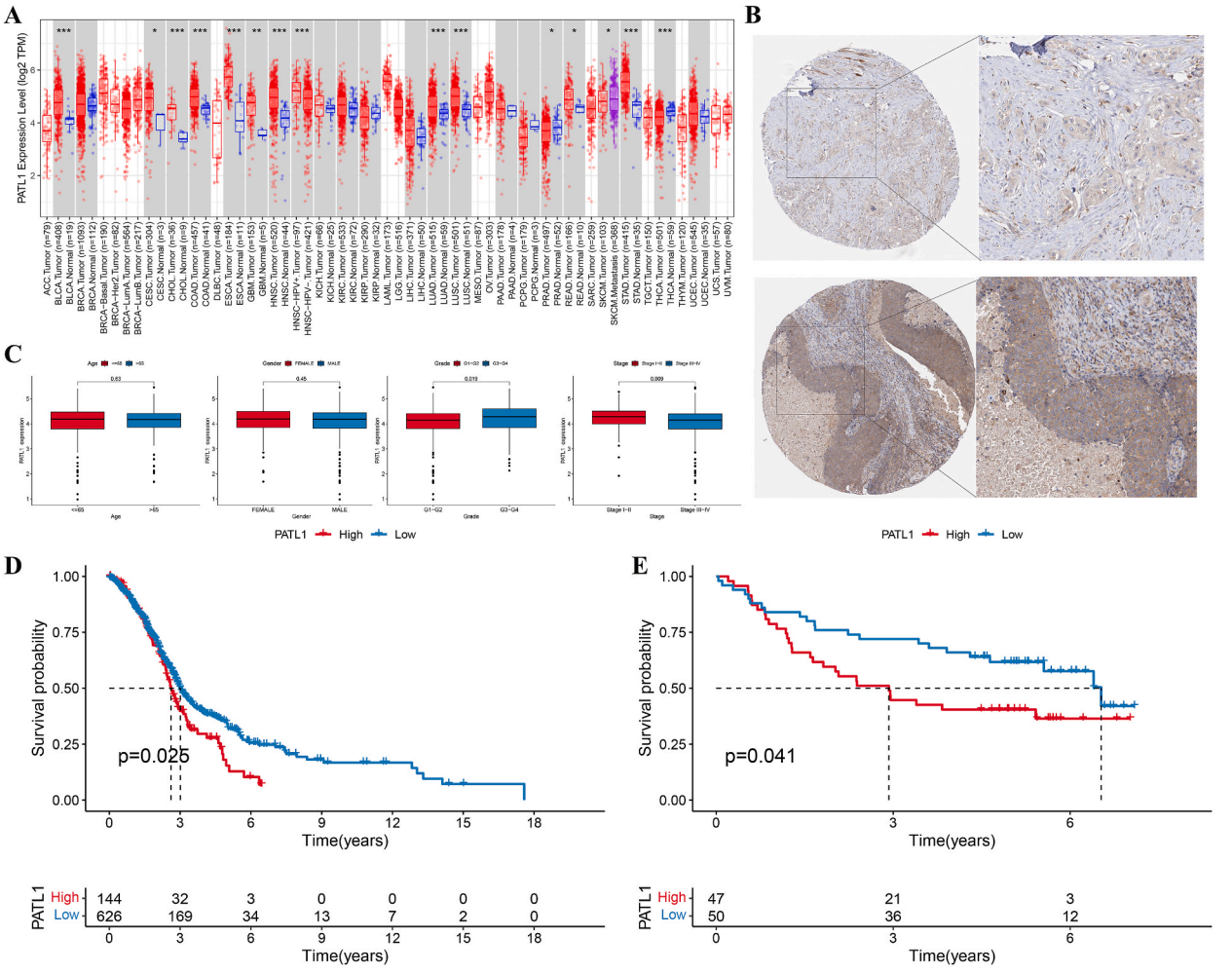

Fig. 5. Role of PATL1 in HNSCC. (A) PATL1 expression levels in pan-cancer. (*$p < 0.05$, **$p < 0.01$, ***$p < 0.001$). (B) Analysis of PATL1 expression in HNSCC by gender, age, and G and TNM stages. (C) Immunofluorescence staining of the PATL1 derived from the HPA database. Up to down: normal tissue, tumor tissue. (D–E) Survival analysis of HNSCC patients in the training set (D) and test set (E). HNSCC: Head and Neck Squamous Cell Carcinoma, HPA: Human Protein Atlas, TNM: Tumor, Node, Metastasis.

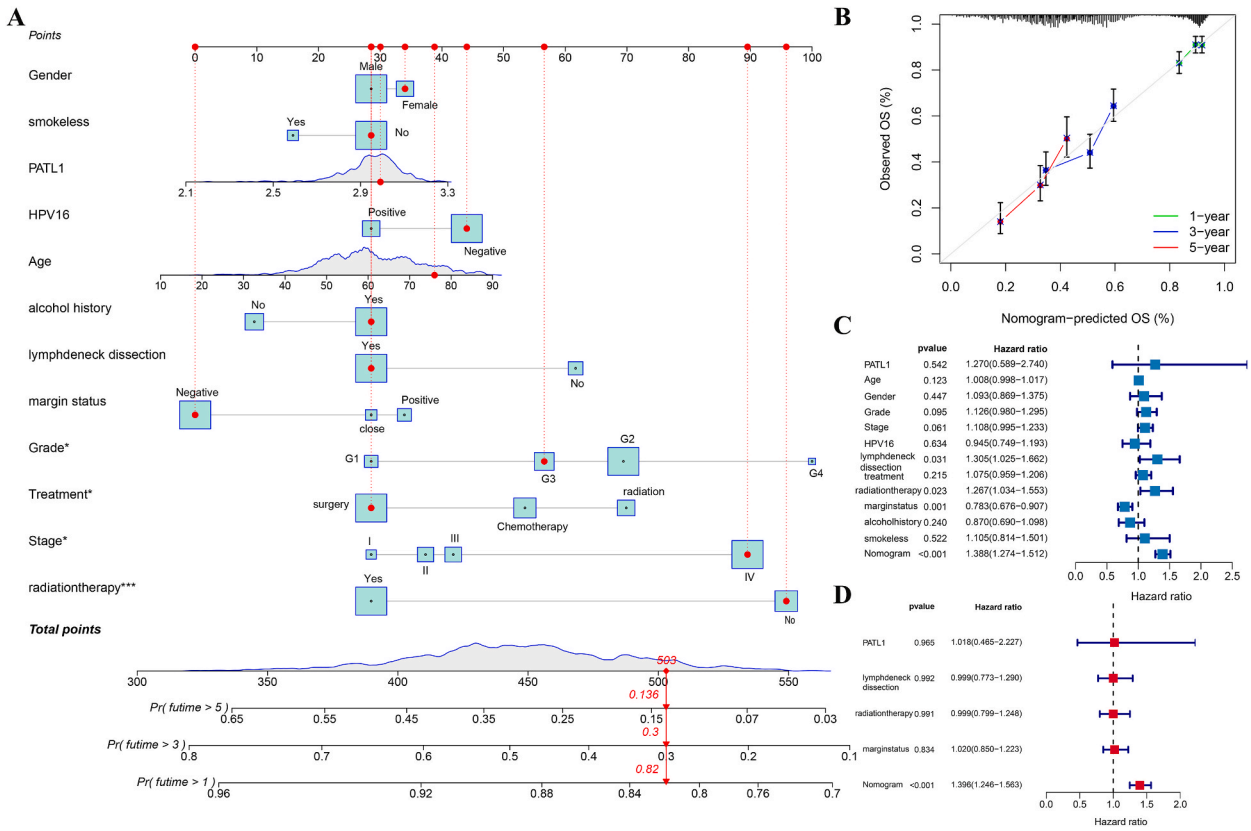

Fig. 6. Prognostic nomogram based on PATL1 expression in HNSCC. (A) A prognostic model in the form of a nomogram to estimate the 1-, 3-, and 5-year overall survival probabilities for individuals diagnosed with HNSCC. (B) Calibration curve illustrating the accuracy of the nomogram in forecasting the 1-, 3-, and 5-year overall survival rates. (C–D) Univariate Cox(C) and multivariate (D)Cox regression analysis of clinical factors and nomogram.

3.4. PATL1 expression correlates strongly with immune function

Given the role of *PATL1* in the prognosis of NKTCL and HNSCC, we further investigated its biological functions. Gene set enrichment analysis (GSEA) showed that *PATL1* activation was linked to cell cycle, apoptosis, and tumor pathways, with metabolic pathways being suppressed (Fig. 7A and B). As immune function and immune cells play important roles in cancer, multiple algorithms showed a close relationship between *PATL1* and various immune cells. For instance, the results of ssGSEA demonstrated a close correlation between *PATL1* and certain anti-cancer immune cells (Fig. 7C). Additionally, examination of TIMER2.0 information indicated a significant connection between *PATL1* levels and the presence of immune cells. The results indicate that *PATL1* could play a role in controlling immune cells and aiding in the advancement of NKTCL and HNSCC. Given the importance of immune checkpoints (ICs) in cancer therapy [29], we also analyzed the relationship between *PATL1* expression and the expression of 48 ICs genes. We examined the relationship between *PATL1* and 23 m6A-related genes, as these genes are essential in the progression and therapy of tumors [30]. The correlation analysis showed a significant relationship between *PATL1* expression and 37 ICs (e.g., *CTLA4*, *PDCD1*) as well as 20 genes related to m6A modification (e.g., *ZC3H13*, *METTL3*) (Fig. 7D–E). Due to the strong correlation between *PATL1* and immune response, we theorized that *PATL1* may be utilized as an indicator for forecasting the effectiveness of immunotherapy. Our hypothesis received support from the findings of TIDE and TCIA analyses, revealing notable disparities in scores between high- and low-expression cohorts (Fig. 8A, B, D, E, G). Microsatellite instability scores, as well as *CTLA4* positive and *PD1* positive scores, were the only factors that did not show significant differences between the two groups (Fig. 8C and F). Taken together, our results indicate that the specific mechanisms underlying the role of *PATL1* in the prognosis of NKTCL and HNSCC are worth exploring further. Moreover, given its close correlation with immune function and the potential for predicting the efficacy of immune therapy, *PATL1* may hold promise as a biomarker for immunotherapy in these cancers.

3.5. PATL1 acts as a potential oncogene in NKTCL and HNSCC

To further clarify the role of *PATL1* in NKTCL and HNSCC, we conducted *in vitro* experiments using the SNK6 and FaDu cell lines. After transfection with siRNA targeting PATL1, Western blot analysis demonstrated that *PATL1* protein levels were significantly

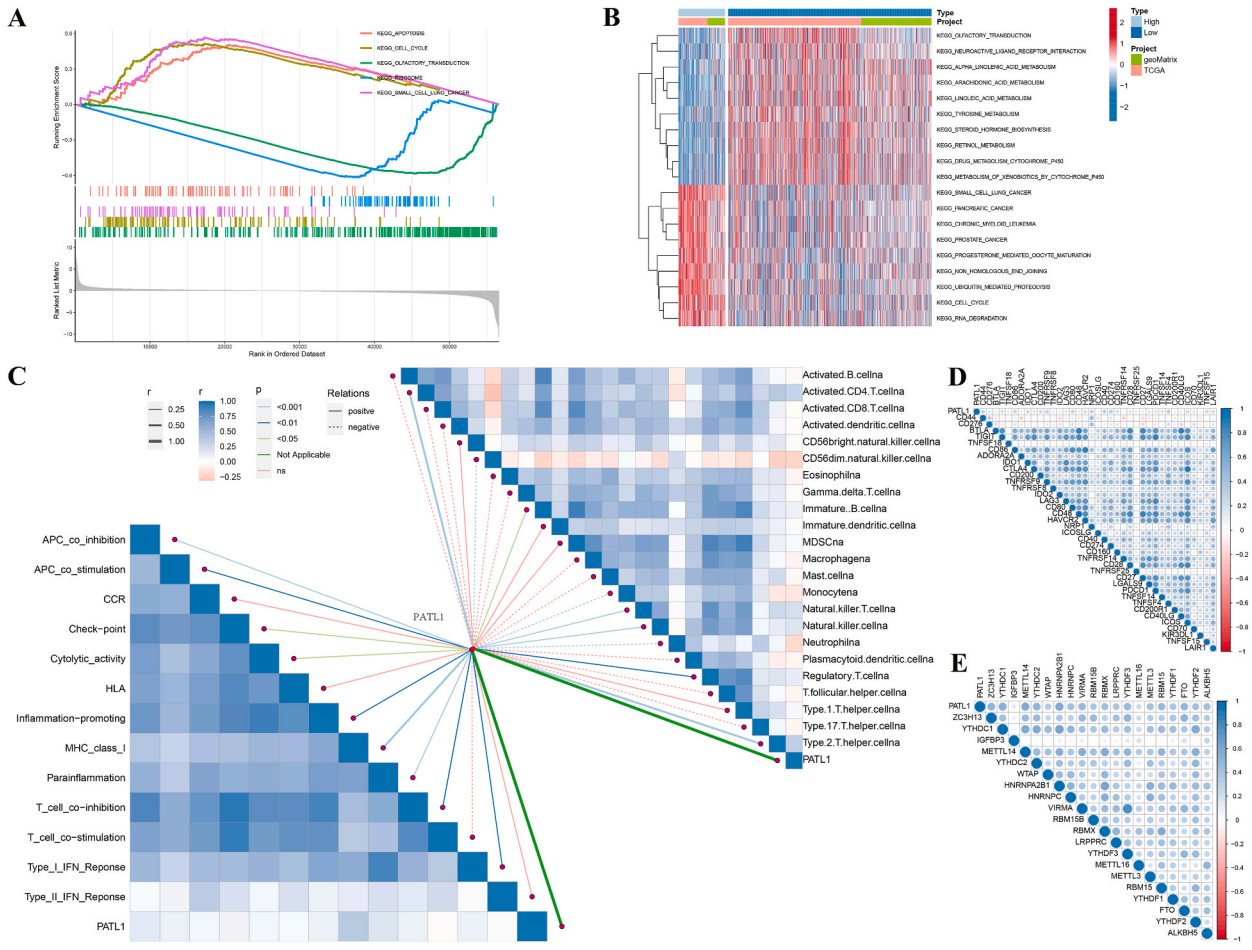

Fig. 7. Biological functions of PATL1. (A–B) Enriched pathways in the high and low-expression PATL1 groups in training cohort. (C) Associations between PATL1, immune-related functions, and the prevalence of each type of immune cell. (D–E) Correlation analysis of PATL1 expression with the expression of 37 immune checkpoints (ICs) (D) and m6A-related genes (E). ICs: Immune Checkpoints, m6A: N6-methyladenosine.

reduced in the si-*PATL1* groups compared to the negative control (NC) and si-NC groups, confirming the efficacy of the transfection (Fig. 9A). CCK-8 indicated a decrease in cellular viability in the si-*PATL1* groups at 2 and 3days post-transfection compared to the control groups (Fig. 9B). Conversely, an increase in cellular apoptosis was observed (Fig. 9C). Additionally, Transwell migration assays revealed a reduction in cell migration following si-P*ATL1* treatment (Fig. 9D). The initial findings from cellular experiments also indicate that *PATL1* could function as a cancer-causing gene in both NKTCL and HNSCC, underscoring its significance as a focus for cancer investigations.

4. Discussion

By analyzing bulk RNA sequencing data from three instances each of NKTCL, nasal polyps, and normal nasal mucosa, along with machine learning techniques, we pinpointed *PATL1* as a central gene. We found that *PATL1* holds significant diagnostic value for NKTCL. Immunohistochemical analysis also showed that patients with high *PATL1* levels in their tumor samples had worse outcomes, indicating that *PATL1* is an independent predictor of prognosis in NKTCL. Additional examination of information from a public database revealed that *PATL1* exhibited increased expression in HNSCC tumor samples, and this heightened level of expression was linked to a poorer prognosis in individuals diagnosed with HNSCC. Additionally, we found a strong connection between the expression of *PATL1* and the presence of different immune cells, along with notable links to the expression of ICs and genes related to m6A modification. The TIDE and TCIA algorithms analysis showed that *PATL1* is predictive of immunotherapy effectiveness in patients with HNSCC. Collectively, these findings suggest that *PATL1* may play a pivotal role in the progression of NKTCL and HNSCC, potentially serving as a valuable prognostic and predictive biomarker, and underscoring its potential as a target for immunotherapy.

The use of bioinformatics to identify diagnostic markers for diseases such as cancer is an increasingly active area of research, as evidenced by previous studies [31,32]. However, similar research in NKTCL is relatively rare. Additionally, most of these studies only analyze gene expression differences between normal and tumor tissues, while we examined differential gene expression in three types

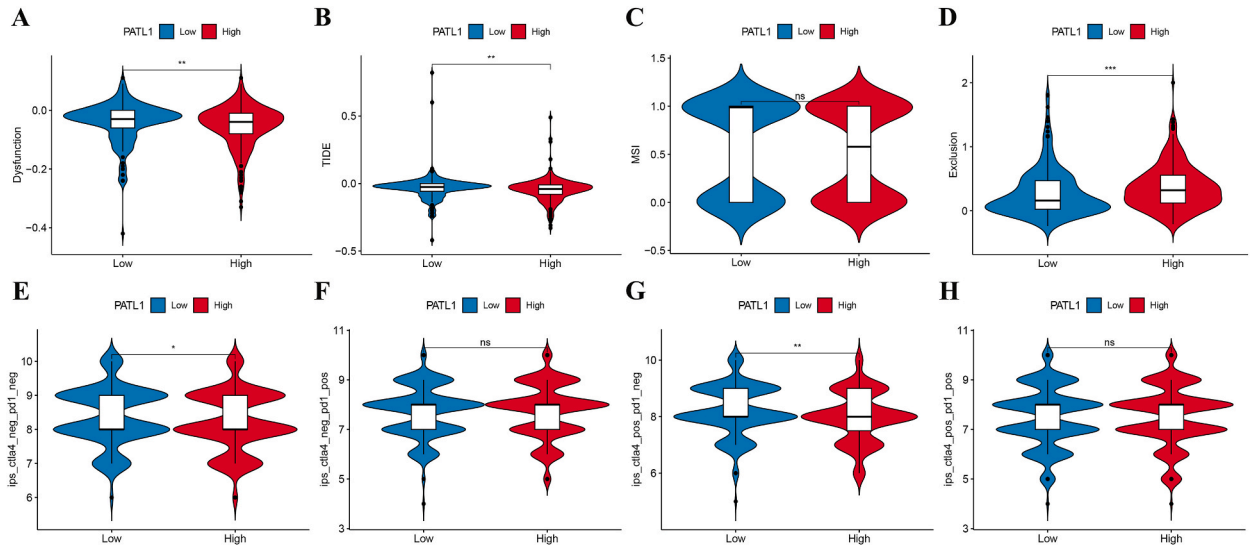

Fig. 8. TIDE and TCIA analysis. (A–D) TIDE analysis of (A) immune dysfunction, (B) tide scores, (C)MSI, and exclusion (D) between low- and high-PATL1 expression groups. (E–H) Differences in the (E) IPS, (F) IPS-CTLA4, (G) IPS-PD1/PD-L1/PD- L2, and (H) IPS-PD1/PD-L1/PD-L2 + CTLA4 between low- and high- PATL1 expression groups. (ns $p > 0.05$, *$p < 0.05$, **$p < 0.01$, ***$p < 0.001$). TIDE: Tumor Immune Dysfunction and Exclusion, TCIA: The Cancer Immunome Atlas, MSI: Microsatellite Instability, IPS: Immunophenoscore, CTLA4: Cytotoxic T-Lymphocyte-Associated Protein 4, PD1: Programmed Cell Death Protein 1, PD-L1: Programmed Death-Ligand 1, PD-L2: Programmed Death-Ligand 2.

of tissue, including NKTCL, nasal polyps, and normal nasal mucosa. This more stringent screening approach may identify biomarkers with higher diagnostic value. Our use of machine learning algorithms identified *PATL1* as a hub gene with high diagnostic value in NKTCL. Despite extensive research on *PATL1* in different biological settings [32], its potential involvement in cancer remains unexplored. This study is the initial one to discuss the significance of *PATL1* in NKTCL and HNSCC, offering fresh potential treatment options for associated genes. Additionally, data from our nearby hospital indicated that *PATL1* is a standalone risk factor for NKTCL. Other studies have reported the prognostic value of some genes in NKTCL [33,34], but we used HNSCC data to confirm that *PATL1* expression is negatively correlated with prognosis across different databases. Nowadays, nomograms are widely used in many bioinformatics studies because they provide a comprehensive and intuitive prediction of clinical performance. However, due to the partially missing information in public databases, these nomograms may not be comprehensive enough. For instance, numerous nomograms have been constructed for HNSCC, incorporating basic clinical data such as age, gender, and TNM staging [35,36].As HNSCC is a highly heterogeneous neoplasm, its prognosis is influenced by a myriad of factors. Building a nomogram based solely on age, gender, and TNM staging would be overly simplistic and neglect the complexity of the disease. Our research is pioneering in utilizing various imputation techniques to address missing data in public databases and incorporating factors like HPV16, treatment approaches, margin status, and lymph node dissection surgery into the nomogram. This provides clinical decision-makers with a more detailed and comprehensive nomogram. Additional examination revealed that the nomogram serves as a standalone predictor for HNSCC outcomes.

Several bioinformatics investigations have examined the predictive significance of specific genes in head and neck tumors like nasopharyngeal carcinoma and HNSCC. However, these analyses typically focused on a single databases, such as TCGA [37,38]. Our study used three datasets, making our results more reliable. In addition, like previous studies [39,40], we also explored the relationship between *PATL1* expression and immune cells infiltration. In NKTCL and HNSCC, there is a strong correlation on between *PATL1* expression and the presence of NKT cells, emphasizing the importance of *PATL1* in NKTCL studies. Furthermore, the potential applications of NKT cell-based immunotherapies in HNSCC underscore the research value of *PATL1* [41]. Additional examination showed that in NKTCL, *PATL1* exhibited a positive association with the presence of nine immune cell varieties, such as macrophages and T cells, which have been thoroughly investigated in studies on lymphoma [42]. *PATL1* expression in HNSCC showed a positive correlation with six immune cells types and a negative correlation with three others. Additionally, analyses based on immune functions indicated that *PATL1* expression was closely associated with the activation of various immune functions, especially CCR and inflammatory responses, highlighting their research value in both NKTCL and HNSCC [43–46]. Therefore, our study emphasizes new strategies for targeting *PATL1* to regulate these immune functions. The immunological studies suggest that *PATL1* may negatively correlate with immune status, potentially leading to poorer outcomes in immunotherapy. Patients exhibiting reduced *PATL1* levels showed decreased TIDE scores in contrast to individuals with elevated expression, providing additional confirmation of our discoveries.

Finally, our cellular experiments further confirmed the oncogenic potential of *PATL1* in NKTCL and HNSCC. However, there are several limitations to our study. First, our RNA transcriptome data from NKTCL patients was limited to only three cases. Considering the variations in lifestyle, environmental factors, age, and gender, future studies should expand the number of transcriptome

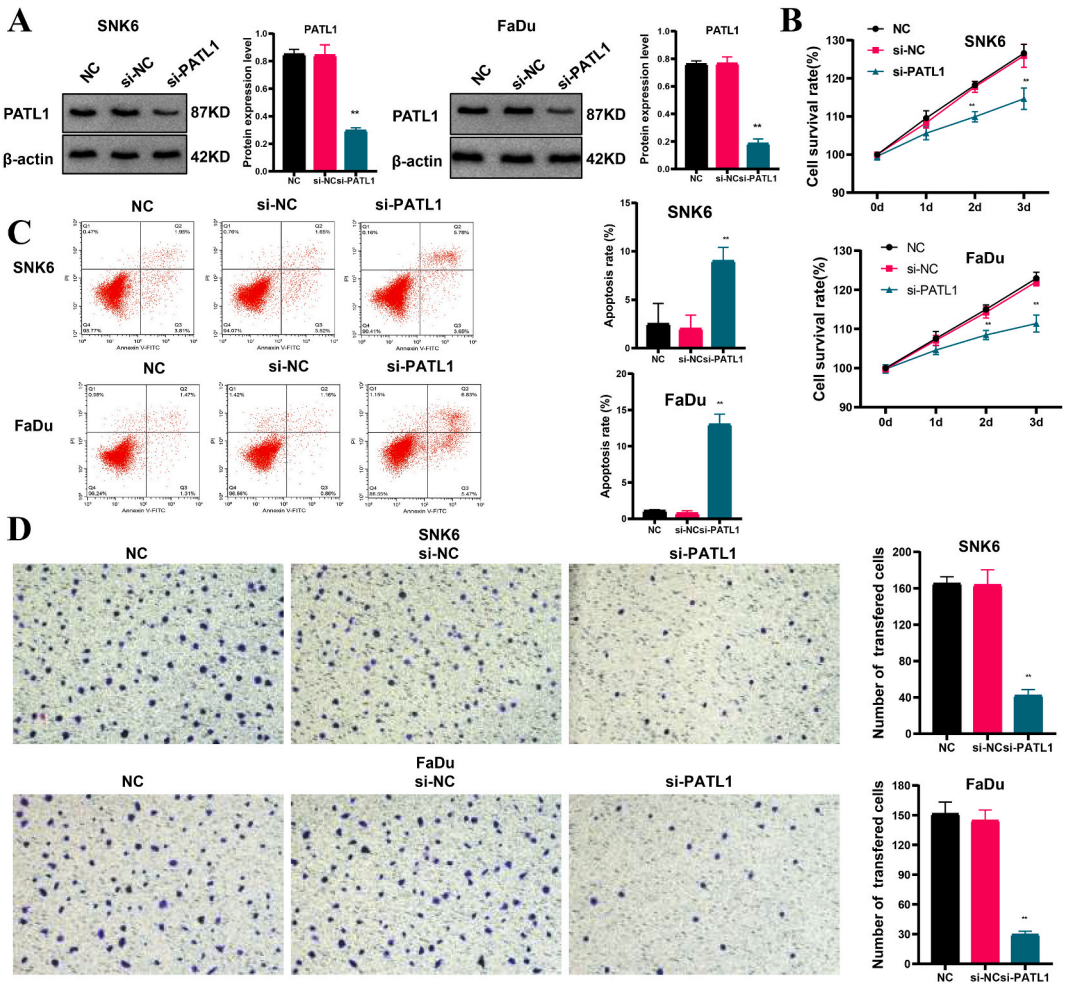

Fig. 9. Effects of siRNA targeting PATL1 on NKTCL and HNSCC cell lines. (A) Western blot analysis showing reduced PATL1 protein levels in SNK6 and FaDu cell lines transfected with si-PATL1.B: Cell viability assays (CCK-8) demonstrate the cellular viability at 0, 1, 2, and 3days post-transfection with si-PATL1 plasmid. (C–D) Flow cytometry and Transwell migration assays illustrate the rates of cellular apoptosis (C) and migration (D) in cell lines post-transfection with si-PATL1 plasmid, respectively. ($^{**}p < 0.01$).

sequencing samples to enhance the generalizability of the research. Second, although we analyzed the prognostic effects of *PATL1* in 55 NKTCL patients, the data originated from a single center, which could introduce bias, and the retrospective analysis might lead to selection bias in the patient cohort. Hence, it is imperative to carry out future prospective studies involving multiple centers. Regarding HNSCC, two major deficiencies were identified: one is the substantial amount of missing data in the training set, which, despite being addressed through multiple imputation methods, could lead to a lack of homogeneity. As the database information is updated and supplemented, we plan to reanalyze the outcomes; the second is that the patients in the TCGA and GEO databases predominantly consist of European descent, which might cause inconsistencies in our findings across different ethnic groups. Thus, more local clinical samples should be collected in the future to improve the reliability and applicability of our results across diverse populations. Moreover, although our initial cellular experiments validated the carcinogenic role of *PATL1* in NKTCL and HNSCC, they did not explore the underlying mechanisms in depth and lacked support from animal studies. Future research should involve more comprehensive experimental work to deeply analyze the mechanisms of tumor formation and development. Finally, we can delve into more sophisticated multi-omics data analysis techniques, including genomics, transcriptomics, and proteomics, in order to enhance our comprehension of the potential molecular pathways linking NKTCL and HNSCC.

5. Conclusion

In summary, *PATL1* seems to be a useful indicator for diagnosing and predicting outcomes in NKTCL and could also act as a prognostic marker and a predictor of response to immunotherapy in HNSCC. In essence, our findings underscore the potential of *PATL1* as a significant tool in the management and treatment of these cancers.

Ethics approval and consent to participate

The study was approved by the affiliated hospital of Guizhou Medical University (2022-121, 2023-527).

Data availability statement

The information provided in this research can be accessed by contacting the author directly with a reasonable request.

Funding

This work was supported by Guizhou Provincial Science and Technology Fund (grant number: [2020] 4Y147).

CRediT authorship contribution statement

Wen Yang: Writing – original draft, Methodology, Conceptualization. **Cong Peng:** Supervision, Project administration. **Zhengyang Li:** Resources, Data curation. **Wenxiu Yang:** Writing – review & editing, Supervision, Funding acquisition, Conceptualization.

Declaration of competing interest

The authors declare that they have no known competing financial interests or personal relationships that could have appeared to influence the work reported in this paper.

Acknowledgements

We are grateful for the assistance from the Guizhou Provincial Science and Technology Fund (grant number: [2020] 4Y147) in supporting this research.

Appendix A. Supplementary data

Supplementary data to this article can be found online at https://doi.org/10.1016/j.heliyon.2024.e32158.

References

[1] H. Sung, J. Ferlay, R.L. Siegel, M. Laversanne, I. Soerjomataram, A. Jemal, F. Bray, Global cancer Statistics 2020: GLOBOCAN estimates of incidence and Mortality worldwide for 36 cancers in 185 Countries, CA. Cancer J. Clin. 71 (2021) 209–249, https://doi.org/10.3322/caac.21660.
[2] Z. Ying, J. Zhu, Extranodal natural killer/T cell lymphoma: we should and we can do more, Chin. Clin. Oncol. 4 (2015) 12, https://doi.org/10.3978/j.issn.2304-3865.2015.03.07.
[3] A. Carbone, A. Gloghini, G. Dotti, EBV-associated lymphoproliferative disorders: classification and treatment, Oncol. 13 (2008) 577–585, https://doi.org/10.1634/theoncologist.2008-0036.
[4] Y.-P. Chen, A.T.C. Chan, Q.-T. Le, P. Blanchard, Y. Sun, J. Ma, Nasopharyngeal carcinoma, Lancet (London, England) 394 (2019) 64–80, https://doi.org/10.1016/S0140-6736(19)30956-0.
[5] S.-B. Ng, J. Yan, G. Huang, V. Selvarajan, J.L.-S. Tay, B. Lin, C. Bi, J. Tan, Y.-L. Kwong, N. Shimizu, K. Aozasa, W.-J. Chng, Dysregulated microRNAs affect pathways and targets of biologic relevance in nasal-type natural killer/T-cell lymphoma, Blood 118 (2011) 4919–4929, https://doi.org/10.1182/blood-2011-07-364224.
[6] P.L. Swiecicki, J.R. Brennan, M. Mierzwa, M.E. Spector, J.C. Brenner, Head and neck squamous cell carcinoma detection and surveillance: advances of liquid biomarkers, Laryngoscope 129 (2019) 1836–1843, https://doi.org/10.1002/lary.27725.
[7] Q. Bi, X. Lian, J. Shen, F. Zhang, T. Xu, Exploration of radiotherapy strategy for brain metastasis patients with driver gene positivity in lung cancer, J. Cancer 15 (2024) 1994–2002, https://doi.org/10.7150/jca.91875.
[8] Q. Bi, Z. Miao, J. Shen, H. Wang, K. Kang, J. Du, F. Zhang, S. Fan, Detecting the research trends and hot spots in external irradiation therapy for rectal cancer, J. Cancer 13 (2022) 2179–2188, https://doi.org/10.7150/jca.69669.
[9] C. Peng, H. Ye, Z. Li, X. Duan, W. Yang, Z. Yi, Multi-omics characterization of a scoring system to quantify hypoxia patterns in patients with head and neck squamous cell carcinoma, J. Transl. Med. 21 (2023) 15, https://doi.org/10.1186/s12967-022-03869-8.
[10] Y. Tang, W. Tian, J. Xie, Y. Zou, Z. Wang, N. Li, Y. Zeng, L. Wu, Y. Zhang, S. Wu, X. Xie, L. Yang, Prognosis and dissection of immunosuppressive microenvironment in breast cancer based on fatty acid metabolism-related signature, Front. Immunol. 13 (2022) 1–17, https://doi.org/10.3389/fimmu.2022.843515.
[11] Z. Mai, H. Chen, M. Huang, X. Zhao, L. Cui, A robust metabolic enzyme-based prognostic signature for head and neck squamous cell carcinoma, Front. Oncol. 11 (2022) 1–12, https://doi.org/10.3389/fonc.2021.770241.
[12] M. Li, H. Ren, Y. Zhang, N. Liu, M. Fan, K. Wang, T. Yang, M. Chen, P. Shi, MECOM/PRDM3 and PRDM16 serve as prognostic-related biomarkers and are correlated with immune cell infiltration in lung adenocarcinoma, Front. Oncol. 12 (2022) 1–15, https://doi.org/10.3389/fonc.2022.772686.
[13] M. Ahmadi, M. Eftekhari Kenzerki, S.M. Akrami, S. Pashangzadeh, F. Hajiesmaeili, S. Rahnavard, L. Habibipour, N. Saffarzadeh, P. Mousavi, Overexpression of HPRT1 is associated with poor prognosis in head and neck squamous cell carcinoma, FEBS Open Bio 11 (2021) 2525–2540, https://doi.org/10.1002/2211-5463.13250.
[14] A.B. Khan, S. Lee, A.S. Harmanci, R. Patel, K. Latha, Y. Yang, A. Marisetty, H.-K. Lee, A.B. Heimberger, G.N. Fuller, B. Deneen, G. Rao, CXCR4 expression is associated with proneural-to-mesenchymal transition in glioblastoma, Int. J. Cancer 152 (2023) 713–724, https://doi.org/10.1002/ijc.34329.
[15] W. Chen, W. Qian, J. Nie, M. Dai, A study of the prognostic value of long non-coding RNA CASC15 in human solid tumors utilizing the Cancer Genome Atlas (TCGA) datasets and a meta-analysis, Clin. Exp. Med. 23 (2023) 65–78, https://doi.org/10.1007/s10238-021-00789-7.

[16] Z. Li, D. Xu, J. Jing, J. Wang, M. Jiang, F. Li, Identification and validation of prognostic markers for lung squamous cell carcinoma associated with chronic obstructive pulmonary disease, JAMA Oncol. 2022 (2022) 4254195, https://doi.org/10.1155/2022/4254195.
[17] S.S.-S. Hue, M.L. Oon, S. Wang, S.-Y. Tan, S.-B. Ng, Epstein-Barr virus-associated T- and NK-cell lymphoproliferative diseases: an update and diagnostic approach, Pathology 52 (2020) 111–127, https://doi.org/10.1016/j.pathol.2019.09.011.
[18] A.A. Gru, J.A. Plaza, J.A. Sanches, D. Miyashiro, O.P. Sangueza, F.B. Puccio, S. Toussaint, J.M. Sangueza, An update on Epstein-Barr virus-and human T-lymphotropic virus type-1-induced cutaneous manifestations. CME Part II, J. Am. Acad. Dermatol. 88 (2023) 983–998, https://doi.org/10.1016/j.jaad.2022.07.063.
[19] K. Manley, J. Dunning, M. Nelson, M. Bower, HIV-associated gastric natural killer/T-cell lymphoma, Int. J. STD AIDS 23 (2012) 66–67, https://doi.org/10.1258/ijsa.2009.009121.
[20] M.J. Koh, M.H. Merrill, M.J. Koh, R. Stuver, C.D. Alonso, F.M. Foss, A.M. Mayor, J. Gill, M. Epeldegui, E. Cachay, J.E. Thorne, M.J. Silverberg, M.A. Horberg, K. N. Althoff, A.E. Nijhawan, K.A. McGinnis, J.S. Lee, C.S. Rabkin, S. Napravnik, J. Li, J.L. Castilho, C. Shen, S. Jain, Comparative outcomes for mature T-cell and NK/T-cell lymphomas in people with and without HIV and to AIDS-defining lymphomas, Blood Adv 6 (2022) 1420–1431, https://doi.org/10.1182/bloodadvances.2021006208.
[21] Y. Zhou, W. Shi, D. Zhao, S. Xiao, K. Wang, J. Wang, Identification of immune-associated genes in diagnosing aortic valve calcification with metabolic syndrome by integrated bioinformatics analysis and machine learning, Front. Immunol. 13 (2022) 1–13, https://doi.org/10.3389/fimmu.2022.937886.
[22] C.-H. Chang, C.-H. Lin, H.-Y. Lane, Machine learning and novel biomarkers for the diagnosis of alzheimer's disease, Int. J. Mol. Sci. 22 (2021), https://doi.org/10.3390/ijms22052761.
[23] Z. Chen, L. Zeng, G. Liu, Y. Ou, C. Lu, B. Yang, L. Zuo, Construction of autophagy-related gene classifier for early diagnosis, prognosis and predicting immune microenvironment features in sepsis by machine learning algorithms, J. Inflamm. Res. 15 (2022) 6165–6186, https://doi.org/10.2147/JIR.S386714.
[24] W.Y. Au, A. Pang, C. Choy, C.S. Chim, Y.L. Kwong, Quantification of circulating Epstein-Barr virus (EBV) DNA in the diagnosis and monitoring of natural killer cell and EBV-positive lymphomas in immunocompetent patients, Blood 104 (2004) 243–249, https://doi.org/10.1182/blood-2003-12-4197.
[25] S.M. Horwitz, S.M. Ansell, W.Z. Ai, J. Barnes, S.K. Barta, M. Choi, M.W. Clemens, A. Dogan, J.P. Greer, A. Halwani, M.H. Bradley, R.T. Hoppe, E. Jacobsen, D. Jagadeesh, Y.H. Kim, M.A. Lunning, A. Mehta, N. Mehta-Shah, Y. Oki, E.A. Olsen, B. Pro, S.A. Rajguru, S. Shanbhag, A. Shustov, L. Sokol, P. Torka, R. Wilcox, B. William, J. Zain, M.A. Dwyer, H. Sundar, T-Cell Lymphomas, Version 2.2018 featured updates to the NCCN guidelines, JNCCN J. Natl. Compr. Cancer Netw 16 (2018) 123–135, https://doi.org/10.6004/jnccn.2018.0007.
[26] M. Shi, J. Du, J. Shi, Y. Huang, Y. Zhao, L. Ma, Ferroptosis-related gene ATG5 is a novel prognostic biomarker in nasopharyngeal carcinoma and head and neck squamous cell carcinoma, Front. Bioeng. Biotechnol. 10 (2022) 1–14, https://doi.org/10.3389/fbioe.2022.1006535.
[27] Z. Xu, B. Peng, Q. Liang, X. Chen, Y. Cai, S. Zeng, K. Gao, X. Wang, Q. Yi, Z. Gong, Y. Yan, Construction of a ferroptosis-related nine-lncRNA signature for predicting prognosis and immune response in hepatocellular carcinoma, Front. Immunol. 12 (2021) 1–13, https://doi.org/10.3389/fimmu.2021.719175.
[28] K. Kang, F. Xie, Y. Wu, C. Han, Y. Bai, J. Long, X. Lian, F. Zhang, Genomic instability in lower-grade glioma : prediction of prognosis based on lncRNA and immune infiltration, Mol. Ther. Oncolytics. 22 (2021) 431–443, https://doi.org/10.1016/j.omto.2021.07.011.
[29] G. Morad, B.A. Helmink, P. Sharma, J.A. Wargo, Hallmarks of response, resistance, and toxicity to immune checkpoint blockade, Cell 184 (2021) 5309–5337, https://doi.org/10.1016/j.cell.2021.09.020.
[30] L. He, H. Li, A. Wu, Y. Peng, G. Shu, G. Yin, Functions of N6-methyladenosine and its role in cancer, Mol. Cancer 18 (2019) 176, https://doi.org/10.1186/s12943-019-1109-9.
[31] S. Zhang, J. Zhang, Y. An, X. Zeng, Z. Qin, Y. Zhao, H. Xu, B. Liu, Multi-omics approaches identify SF3B3 and SIRT3 as candidate autophagic regulators and druggable targets in invasive breast carcinoma, Acta Pharm. Sin. B 11 (2021) 1227–1245, https://doi.org/10.1016/j.apsb.2020.12.013.
[32] L. Liu, Z. Liu, J. Gao, X. Liu, S. Weng, C. Guo, B. Hu, Z. Wang, J. Zhang, J. Shi, W. Guo, S. Zhang, CD8+ T cell trajectory subtypes decode tumor heterogeneity and provide treatment recommendations for hepatocellular carcinoma, Front. Immunol. 13 (2022) 1–17, https://doi.org/10.3389/fimmu.2022.964190.
[33] J. Liu, L. Liang, S. Huang, L. Nong, D. Li, B. Zhang, T. Li, Aberrant differential expression of EZH2 and H3K27me3 in extranodal NK/T-cell lymphoma, nasal type, is associated with disease progression and prognosis, Hum. Pathol. 83 (2019) 166–176, https://doi.org/10.1016/j.humpath.2018.08.025.
[34] Q. Ye, H. Chen, Z. Wen, W. Guo, Y. Huang, X. Mo, Abnormal expression of p-ATM/CHK2 in nasal extranodal NK/T cell lymphoma, nasal type, is correlated with poor prognosis, J. Clin. Pathol. 74 (2021) 223–227, https://doi.org/10.1136/jclinpath-2020-206476.
[35] Y. Lu, Z. Jia, Inflammation-related gene signature for predicting the prognosis of head and neck squamous cell carcinoma, Int. J. Gen. Med. 15 (2022) 4793–4805, https://doi.org/10.2147/IJGM.S354349.
[36] Z. Mai, H. Chen, M. Huang, X. Zhao, L. Cui, A robust metabolic enzyme-based prognostic signature for head and neck squamous cell carcinoma, Front. Oncol. 11 (2022), https://doi.org/10.3389/fonc.2021.770241.
[37] G. Liu, X. Zeng, B. Wu, J. Zhao, Y. Pan, RNA-Seq analysis of peripheral blood mononuclear cells reveals unique transcriptional signatures associated with radiotherapy response of nasopharyngeal carcinoma and prognosis of head and neck cancer, Cancer Biol. Ther. 21 (2020) 139–146, https://doi.org/10.1080/15384047.2019.1670521.
[38] Y. Ouyang, Y.B. Jin, X.P. Chen, G.Y. Zhang, S.L. Mao, F. Ling, W. Luo, STIL is upregulated in nasopharyngeal carcinoma tissues and promotes nasopharyngeal carcinoma proliferation, migration and invasion, Neoplasma 67 (2020) 37–45, https://doi.org/10.4149/neo_2019_190306N192.
[39] T. Wang, N. Dang, G. Tang, Z. Li, X. Li, B. Shi, Z. Xu, L. Li, X. Yang, C. Xu, K. Ye, Integrating bulk and single-cell RNA sequencing reveals cellular heterogeneity and immune infiltration in hepatocellular carcinoma, Mol. Oncol. 16 (2022) 2195–2213, https://doi.org/10.1002/1878-0261.13190.
[40] G.L. Zhu, K. Bin Yang, C. Xu, R.J. Feng, W.F. Li, J. Ma, Development of a prediction model for radiotherapy response among patients with head and neck squamous cell carcinoma based on the tumor immune microenvironment and hypoxia signature, Cancer Med. (2022) 1–15, https://doi.org/10.1002/cam4.4791.
[41] F. Ihara, S. Motohashi, [Invariant NKT cell-based immunotherapy for lung cancer and head and neck cancer], Nihon Rinsho 75 (2017) 312–316.
[42] I.E. Galani, M. Wendel, A. Stojanovic, M. Jesiak, M.M. Müller, C. Schellack, E. Suri-Payer, A. Cerwenka, Regulatory T cells control macrophage accumulation and activation in lymphoma, Int. J. Cancer 127 (2010) 1131–1140, https://doi.org/10.1002/ijc.25132.
[43] Z. Wang, K.L. Kirkwood, Y. Wang, W. Du, S. Lin, W. Zhou, C. Yan, J. Gao, Z. Li, C. Sun, F. Liu, Analysis of the effect of CCR7 on the microenvironment of mouse oral squamous cell carcinoma by single-cell RNA sequencing technology, J. Exp. Clin. Cancer Res. 43 (2024) 94, https://doi.org/10.1186/s13046-024-03013-y.
[44] C.-C. Wang, M.-H. Hsu, C.-T. Lee, C.-J. Chen, T.-Z. Hwang, H.-P. Wang, J.-T. Lin, W.-L. Wang, Prognostic significances of systemic inflammatory response markers in patients with synchronous esophageal and head and neck cancers, Head Neck (2024), https://doi.org/10.1002/hed.27677.
[45] I. Omori, H. Kamijo, H. Suga, T. Miyagaki, K. Taoka, K. Toyama, M. Kurokawa, S. Sato, Extranodal natural killer/T-cell lymphoma, nasal type with CCR3 and CXCR3 expression, Clin. Exp. Dermatol. 45 (2020) 608–610, https://doi.org/10.1111/ced.14181.
[46] Y.-J. Li, W.-Q. Jiang, J.-J. Huang, Z.-J. Xia, H.-Q. Huang, Z.-M. Li, The Glasgow Prognostic Score (GPS) as a novel and significant predictor of extranodal natural killer/T-cell lymphoma, nasal type, Am. J. Hematol. 88 (2013) 394–399, https://doi.org/10.1002/ajh.23422.